Use of numerical simulation to map and mitigate railway particle emissions

Peter Torstensson

Tore Vernersson

Sara Janhäll

Anders Andersson

Fredrik Blennow

Kristoffer Mossheden

Abstract

This feasibility study is an interdisciplinary collaboration between three research institutes (VTI, Chalmers University of Technology and RISE) and a railway brake manufacturer (Faiveley Transport Nordic). Senior researchers specialized on numerical modelling of friction brakes and on particle matters (PM), are combined with expertise in the field of train driving simulation to reduce railway's impact on environment and human health. The train driving simulator of VTI is further developed to account for the wear generated at the brake blocks and in the wheel–rail contact. A literature study that focuses on prediction of railway particle emissions is presented. The literature shows effects on particle emission from relative velocity between the mating surfaces, temperature in the surfaces and pressure between the surfaces. A large part of the reported particle data does not include the coarser (i.e. larger) particles and use different definitions to describe particle diameter. Still, the information found give an indication of a first attempt to divide the wear volume into particle emissions. The new functionality for prediction of wear generation is demonstrated for the railway line between cities Forserum – Tenhult – Huskvarna – Jönköping located in the province Småland, Sweden. A freight train of 619 m length with a total mass of 2 782 tonnes is simulated. Results obtained for an experienced driver is compared to those simulated with an aggressive train driving behavior that activates the Automatic Train Control (ATC) system. The worn off mass generated in the wheel–rail contacts for the latter is found to be approximately 38 % larger compared to that by the experienced driver. Similarly, the wear of the brake blocks is found to be 81 % larger for ATC braking than for braking by an experienced driver. The project has received financial support from the strategic innovation program InfraSweden2030 jointly financed by Vinnova, the Swedish energy agency and the Swedish research council Formas.

Preface

This is the final report from project "Train driving simulation as a tool to reduce railway particle emissions" that has formed part of the activities in the strategic innovation program InfraSweden2030 jointly financed by Vinnova, the Swedish energy agency and the Swedish research council Formas. According to the structure of InfraSweden2030, the current work constitutes a pre-study ("genomförbarhetsstudie") with the aim to form basis for a subsequent application for a so-called Research and Innovation project ("forsknings och innovationsprojekt"). The work has been a joint effort by Anders Andersson, VTI, Fredrik Blennow, Faiveley Transport Nordic, Sara Janhäll, RISE, Kristoffer Mossheden, Faiveley Transport Nordic, Peter Torstensson, VTI, and Tore Vernersson, Chalmers. The advices and train simulations by Niklas Olsson and Thiago Cavalcanti of VTI are acknowledged. Kristoffer Jäsperi of VTI developed and implemented the method for visualization of prediction results. Peter Torstensson, VTI, has been project leader.

Gothenburg, February 2019

Peter Torstensson
Project leader

Table of content

1.   Background

The Swedish Transport Administration, Trafikverket, predicts an increase in the transportation work for all modes of transportation by 50 percent until 2040 [1]. This development is driven by the request for sustainable transportation from industry and an increasing population. Urbanization makes people settle in regions restricted to the larger cities including commuter areas and parts of the countryside with close access to transportation hubs [2]. The importance of the transportation system for house building and in the creation of sustainable and attractive city environments has been recognized by the government [3]. To accommodate the future transportation demand, Trafikverket has suggested actions to increase the capacity of the existing railway infrastructure as well as the building of new track [4]. As an example of the former, actions to double the capacity of the harbor line of Gothenburg is planned. At several sections the current track alignment is close to housing areas and urban centers. The potential construction of approximately 1 500 km new high-speed railway track should also be noted.

The health effects of particle emissions on urban population is a major concern. This is for example demonstrated by its high health cost as compared to that due to gas emissions in Trafikverkets economical model ASEK [5]. The health impact is determined by the particle size, morphology and content. The available literature on particle emissions from railways is limited compared to that for road vehicles. To reduce the influence from weather and other environmental conditions, particle emissions from railways have primarily been investigated for traffic in tunnels. The arrival of a train at a station platform has been measured to correspond to a fivefold increase in particle concentration. Large differences in particle concentrations have been measured for different train individuals [6], as well as in a comparison between passenger and freight trains [7]. In [8] braking is measured to generate one third of the total amount of particles emitted from railways.

Tread braking is the conventional braking system of freight trains. The application of the brake block onto the wheel tread induces a braking force on the wheelset which in turn is transmitted to the wheel–rail contact. In Sweden the most common material used for brake blocks is cast iron. Braking with cast iron brake blocks induces wear to both the brake block and wheel tread. The extent of the wear is influenced by the brake block material and the operative conditions in combination with the behavior of the driver. In particular, the temperature developed in the brake block–wheel contact during braking affects the materials' resistance to wear. Different brake block materials show a varying nonproportional increase in worn off material at elevated temperatures. This temperature dependency is by large governed by the brake block material used. An increase in temperature may also influence the size and morphology of the emitted particles. Braking with cast iron brake blocks promotes growth of out-of-roundness on the wheel tread which results in an increased radiation of rolling noise. In addition, tread braking with cast iron brake blocks are prone to generate squeal noise. These noise issues are the primary reasons for the ongoing development of alternative brake block materials such as sinter materials or organic composites materials.

While enabling a stable vehicle running behavior at high speeds, the attachment of a wheelset to a bogie frame through the primary suspension may result in a deteriorated steering ability on curves. As a result, tangential forces and associated relative sliding develop in the wheel–rail contacts which subsequently introduce wear (e.g. of the wheel flange) and sometimes also damage in the form of rolling contact fatigue (e.g. cracks at the gauge corner of the high rail). The wheelset steering behavior deteriorates significantly if a tractive or braking moment is applied [9]. The UIC-project EuropeTrain studied the damage of brake blocks and wheel treads of two different types of LL-blocks (brake blocks specifically developed to retrofit cast iron brake blocks) and cast iron brake blocks. The wear on the wheel treads caused by the LL-blocks were observed to exceed that generated by the cast iron brake blocks. Moreover, the wheel tread wear introduced by the LL-blocks was found to increase the effective conicity and hence to affect the vehicle steering behavior. This is a safety issue that can lead to unstable running at high vehicle speeds. The altered wheel profile geometry may also have an undesirable influence on the vehicle curving behavior giving rise to exaggerated damage on wheels and rails.

In the current work, researchers at the national road and transport research institute (VTI), Chalmers University of Technology and Research institutes of Sweden (RISE) collaborate with a world leading manufacturer of brake equipment (Faiveley Transport Nordic) to reduce the environmental and health effects of railway transportation. Computational efficient models for prediction of wear in the brake block–wheel and wheel–rail contacts are developed at Chalmers and VTI, respectively. Both are applied in a post-processing step to the train driving simulator of VTI. The possibility for it to be applied during real-time train simulation is discussed and a procedure to accomplish that is described. The state of knowledge on methods to predict particle emissions is presented in a literature study.

2. Aim

This study intends to combine knowledge about generation of material damage in the form of wear with that on particle emissions, and to make the results of this research effort relevant by applying it in conjunction with the train driving simulator. The ultimate purpose of the work is to reduce the railway's effect on the environment and the human health. The current project forms basis for future research efforts in the current area of knowledge.

A procedure to predict the wear generated in the brake block–wheel and wheel–rail contacts caused during simulation in the train simulator is to be developed and demonstrated. The method is applied to assess the importance of the train driving behavior with respect to the generated amount of wear. The state of knowledge on methods to predict particle emissions is presented in a literature study.

3.   Particle size distributions

The relation between the mass of the calculated wear and the emissions of particles depends on the particle size distributions and on the morphology of the particles. The particles in focus are small enough to stay floating in the air and for direct health aspects also small enough to enter the breathing system of human beings. Environmental effects, on the other side, can be found also for larger particles, as they easily move material from the worn surfaces to the surroundings, they either fall down close to the railway track or blow away large distances from it. This might result both in soiled surfaces, esthetical and practical problems, and on pollution of the environment.

In this chapter aerosol physics and particle definitions are shortly described, followed by a description of the specific literature on air quality close to railway track and on emission measurements performed both in field and in laboratory. Focus is on brake–wheel and rail–wheel mechanical systems.

3.1.   Particle characteristics

Particle concentrations related to environmental air quality protection is measured as PM_{10} or $PM_{2.5}$. These measures are defined in the literature, and in principle give the mass of all collected particles smaller than 10 or 2.5 µm in diameter. The limits are chosen to exclude the particles that are too large to enter the human breathing system (PM_{10}) and large enough to enter into the lungs ($PM_{2.5}$). The regulation focuses on mass of particles and does not differentiate between particles of different content or morphology, even if these variables do affect the health outcome to a large extent. Also, the number of particles is important to the health outcome, and the particle number are increasingly easy to measure with modern analyzing equipment, but legislation is still on mass of particles.

To give a view of the effect of particle size a 10 µm particle (i.e. the largest particle included in PM_{10}) is divided into 0.5 µm particles. Instead of one single particle this makes 8000 particles. These smaller particles also penetrate further into the breathing system than most coarser particles and might thus have a larger health outcome. Particles can also be much smaller than 0.5 µm, or even larger than 10 µm. Particles larger than 10 µm diameter are not included in the definitions of air quality particle measures, and thus often not measured.

In the European Union the limit values of PM_{10} concentrations in air where humans are breathing is 40 µg/m^3 as a yearly average and 50 µg/m^3 as a daily average. This is allowed to be exceeded during a maximum of 35 days a year. For $PM_{2.5}$ the limit value is 25 µg/m^3 as a yearly average combined with an extra demand on decreasing exposure of the public. Most Swedish communities have lower values as guideline and target values, and there are also lower values combined with demands on more evaluation of the air quality situation. The target values of particle air pollution are presently difficult to achieve in many Swedish communities, and as effects on human health are shown even for concentrations below these target values, there is an ongoing work to limit the emissions of particles to ambient air.

Particles larger than 10 µm in diameter are not included in the environmental legislation, but still affect soiling and dispersion of the worn material. The smaller these particles are the further away from the source they are transported. Thus, alloys of rare metals that have a larger environmental effect than iron must be discussed in the context of wear particles larger than 10 µm.

The particles emitted from railways are mainly metal wear particles and the health effect of these particles has been compared to effects from road dust. This comparison showed that railway particles are more genotoxic than road dust [10], while road dust was more inflammatory than subway wear particles [11]. Thus, the health outcome differs between the two, but one cannot be valued as more harmful compared to the other as they affect different parts of the body.

3.1.1. Particle diameters

Particle size is often given as the diameter. The particle diameter is defined in different ways as most particles are not spherical and as such does not have one specific and defined diameter. For legislation purposes only PM_{10} and $PM_{2.5}$ are properly defined, and thus particle diameter definitions vary and depend on the type and setting of the instrument that performs the measurements. The particle size also affects how far the particles are spread from the point of emission, and thus, if the distance is critical the need of knowing which diameter to use becomes important. The most common diameters used are aerodynamic diameter (Stokes diameter), electrical mobility diameter, optical diameter and equivalent diameter. The latter is the one that describes the amount of material needed to form the particle, i.e. the diameter that can be related to the amount of material worn from the surfaces. This type of diameter is very seldom measured, and instead the diameter measured depends on the type of instrument. If both the aerodynamic diameter and the electrical mobility diameter are measured the efficient diameter can be determined given that the density of the particle material is known.

The aerodynamic diameter depends of the falling velocity of the particle and is the diameter of a sphere with unit density falling at a velocity that corresponds to that measured. This diameter is calculated as:

$$v_{\mathrm{a}} = \frac{\rho d_{\mathrm{a}}^2 g C_{\mathrm{c}}}{18\eta} \tag{1}$$

where v_{a} is the falling velocity of the particle, ρ is the material density (typically set equal to one), d_a is the particle diameter, g is the gravitational acceleration, C_c is the Cunningham correction factor and η is the viscosity of air. The Cunningham correction factor is used for particles smaller than 1.5 μm. This diameter is also often used in the form of the Stokes diameter where the actual density of the material of the particle is used. Stokes diameter is thus approximately one third of the aerodynamic diameter if the particle is a spherical iron particle, i.e. with an approximate density of 8 g/cm³.

The electrical mobility diameter, d_{m}, is calculated from the velocity of a charged particle (n number of elemental charges e) in an electrical field, E:

$$v_{\mathrm{e}} = \frac{neEC_c}{3\pi\eta d_{\mathrm{m}}} \tag{2}$$

Thus, as we can see from Equations (1)-(2), the relation between the velocity and the diameter differs. Moreover, the material density of the particle is not included in the electrical mobility diameter, see Equation (2). In this way the diameter of all spherical particles can be related to each other. Still, different shapes complicate the picture. Often the shape is described experimentally by a shape factor, χ, included in the equations, e.g.:

$$v_{\mathrm{a}} = \frac{\rho d_{\mathrm{a}}^2 g C_{\mathrm{c}}}{18\eta\chi} \tag{3}$$

There are also different optical diameters used, and those normally depend to a large extend on the kind of aerosol used for calibration, as optical absorption, refractive index and other optical parameters.

The particles in focus here mainly consist of metals, as the worn material originate from wheels, rails or brake blocks. However, the brake blocks can be manufactured by other types of materials such as sinter or organic composites. The shape of the particles also affects the equivalent diameter, i.e. if the particles are melted and reformed in the air, they are often close to spherical and thus less problematic compared to wear flake particles. For those particles the shape factor can be more than double of the shape factor for the sphere [12].

3.2.   Railway non-exhaust particle emissions

The data on wear particles emitted from railway traffic is obtained from the same type of measurements as for normal wear studies but combined with measurements of particle concentrations. There is also some data on particle concentrations from tunnel or station environments. This can be used for comparisons against data from experimental wear tests. Still, the amount of available data is limited. Laboratory wear tests are typically performed in pin-on-disc, twin-wheel or brake rig experimental setups. Particle data is obtained either from closed environments around the mating surfaces, or close enough to the mating surfaces to limit the problem with unknown dilution of the emissions.

During braking, the normal contact pressure varies locally within the brake block–wheel contact area. At least in the beginning of a brake cycle the sliding velocity is high. For wheel–rail contact the speed difference between surfaces in contact during rolling is small. For cases with large magnitude sliding in the wheel–rail contact the wear is often of catastrophic type [13]. This also influences the temperature of the mating surfaces, which has a large influence on the particle characteristics.

At high temperatures and large relative velocity between the contacting surfaces, ultrafine particles are emitted while at large contact pressures and low speeds coarse particles are emitted [14]. For a doubling in relative velocity the particle number density can increase 2-3 times [15] or even more [16]. In addition, there is a transient development during braking, i.e. the particle sizes differ between the first and later part of the braking cycle, assumed to be related both to a difference in temperature and to mechanical material effects on the mating surfaces.

From pin-on-disc tests the most common particle size is close to 350 nm [17]. Nanoparticles can also be emitted at low temperatures and then be a result of cracking of the extremely thin oxidative layer on the surface, as temperatures are not often high enough to give nanoparticles due to heat. At higher temperatures, i.e. above 50˚C, the ultrafine particles, i.e. 15-65 nm are not seen, while most particles are around 150 nm. For lower sliding speeds, the ultrafine particles are emitted in the beginning of the test before heating up the surfaces (up to 35˚C) [16].

Most studies do not include the particles larger than PM_{10}, and as these particles can be very large as compared to even a large number of e.g. ultrafine particles, the relation between wear volume and particle numbers is always rather uncertain and needs more data to be more than a qualified guess.

3.3.   Numerical prediction

This literature review is based on between 40 and 50 papers, including both studies on other brake emissions than railways, and papers including only limited particle information. Most of the work that is directly related to the research question is by the research group under Professor Ulf Olofsson at the Royal Institute of Technology (KTH), Sweden, that has a long history of measurements of railway wear particles.

The variation of different situations when wear is caused during train operation is vast and neither field nor experimental data is sufficient to enable prediction of the emitted wear particles. The qualified guess that is the result of this study is still that a large portion of the particles are close to 350 nm in diameter, and for particle numbers, around 20 % might be 2-4 μm in diameter. The number of ultrafine particles emitted in the size range below 80 nm has a weak relation to the total worn-off volume. This is due to the small total volume of the ultrafine particles. Instead the temperature developed in the contact between the sliding surfaces is believed to be important with respect to the emissions of ultrafine particles.

Studies on non-exhaust particle emission to improve the understanding of emission factors for particles of different sizes and morphology are recommended. The relation between worn material volume and PM_{10} should be investigated as some particles might be larger than 10 μm. Until this data is available the first assumption of wear particle emissions might be that the emissions are present in four modes,

i.e. 80 nm, 350 nm, 3 µm and 20 µm (the last group is above 10 µm in diameter and thus not included in air quality measurements). It is assumed that particles of size 80 nm are only emitted when the temperature in the contact between the mating surfaces is above 50˚C and exposed to a speed larger than 5 m/s. For particles larger than PM_{10} it is suggested that 10 % respective 90 % of the wear volume is divided into similar number of particles of 350 nm and 3 µm. The used particle diameter is Stokes, i.e. the aerodynamic diameter but with iron as the density of the particles.

4.   Train driving simulator

VTI today hosts "Tågsimulator UtvecklingsForum För Användare (TUFFA)" with members among train operators (e.g. SJ, MTR, Green Cargo) as well as railway educational institutions (Järnvägsskolan, Nässjöakademin och TCC). In TUFFA the train simulators are further developed in accordance with the members' desires. This includes which railway lines, vehicle types and scenarios to implement. Results are shared and discussed in reoccurring meetings in the group. Today, among others, a train powered by a Bombardier TRAXX locomotive has been implemented. Below follows a brief description of this vehicle model. In Section 4.2, a procedure for it to be applied in a co-simulation setup in which material damage is calculated in real-time with models located on external separate computers is discussed.

4.1.   The freight train simulator

The train simulator of VTI consists of three major modules; (1) the train driver environment potentially including a physical instrument layout, (2) a vehicle dynamics model and (3) a model for the infrastructure including an integrated signaling system. A realistic track alignment is modelled based on Trafikverket's "track information database" (BIS). The software accounts for the Automatic Train Control (ATC) system. Below the train dynamics model is presented. A more detailed description is found in [18].

The freight train model has a modular structure that allows for an arbitrary number and configuration of locomotives and freight wagons. Driving torque is only applied on the wheel of the locomotive(s). Further, only the locomotives feature an electrodynamic brake that enables to use the motor to apply a braking moment on the wheelset. For all wagons of the train set a pneumatic braking system is modelled. Each wagon is described as a single wheel with rotational inertia, J_i, calculated as the sum of the rotational inertia of the included wheelsets, see Figure 1. The wheel has radius r_i and angular rotational speed ω_i. A vertical static load, $m_i g$, is applied on the wheel, where m_i is the unit summed mass of both the wagon and cargo and $g = 9.81$ m/s^2 is the gravitational constant. Vehicle speed is v. The equation of motion of the train in tangential translation, and for wheel i in rotation, are obtained as:

$$\dot{v} \sum_i m_i = -F_A + \sum_i F_{T,i} - F_{S,i} - F_{C,i} - F_{eB,i} \tag{4}$$

$$\dot{\omega}_i J_i = T_{D,i} - T_{pB,i} - T_{R,i} \tag{5}$$

The air resistance force, F_A, is calculated for the whole train and depends on the locomotive front area and the train total length. Tangential forces applied on wheel i due to vertical gradients, $F_{S,i}$, rolling resistance on curves, $F_{C,i}$, wheel–rail contact, $F_{T,i}$, and electrodynamic braking, $F_{eB,i}$, are expressed as:

$$F_{S,i} = m_i g \theta \tag{6}$$

$$F_{C,i} = m_i \frac{k_C}{r_C - 55} \tag{7}$$

$$F_{T,i} = m_i g f(\mu, s) \tag{8}$$

$$F_{eB,i} = \begin{cases} \zeta 150 \cdot 10^3 & \text{if } v < 10 \text{ km/h} \\ 15\zeta v & \text{if } v > 10 \text{ km/h} \end{cases} \tag{9}$$

where θ is the vertical gradient expressed as an angle of inclination, k_C is a constant determined by the bogie construction, r_C is the curve radius and ζ is the braking demand by the driver varying in the range between 0 and 1. Equation (8) shows how the tangential wheel–rail contact force is calculated dependent

on the non-linear function $f(\mu,s)$, where μ is the friction coefficient and s is the relative slip between wheel and rail. For details see [18].

Moments applied on the wheel to account for the pneumatic braking system, $T_{pB,i}$, and rolling resistance, $T_{R,i}$, are expressed as:

$$T_{pB,i} = m_i g \alpha r_i \frac{5 \cdot 10^5 - p_i}{1.5 \cdot 10^5} \tag{10}$$

$$T_{R,i} = m_i r_i (c_1 + c_2 v) \tag{11}$$

Where p_i is the air pressure in the main pipe of wheel i, α is the maximum allowed brake utilization here set to 0.1, and $c_1 = 0.015$ m/s^2 and $c_2 = 0.0002$ s^{-1} are measured constants. The applied driving torque, $T_{D,i}$, on wheel i accounts for a traction control system implemented using a PI-controller [18]. Mainly due to air flow resistance, the pneumatic brake system introduces a time delay affecting the operation of the train. In the current work, the pressure distribution in the main braking pipe is modelled as a diffusion process in accordance with [19]:

$$\frac{\partial p}{\partial t} = \beta p \frac{\partial^2 p}{\partial x^2} \tag{12}$$

where β is the dynamic air flow resistance. The partial differential equation of Equation (12) is converted into a system of ordinary differential equations and solved with an implicit Euler method. For the first and last unit a slightly different equation is used. A more detailed description is found in [19].
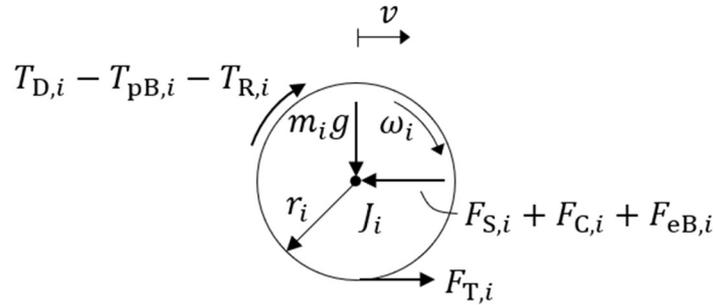
Figure 1. The vehicle model used in the train simulator

4.2.   Co-simulation and train driver feedback in real-time

Co-simulation between the train simulator and the tools for estimating the particle emissions and material damage requires them to be connected and have support for communication. Thus, instead of post-processing data, the data is sent in real-time from the train simulator to the models for particle emission and material damage. These models calculate and send back their results to the train simulator where they can be displayed to the train driver. This solution requires communication infrastructure and interfaces but allows for the different models in the procedure to be distributed at different physical locations. As such, in this setup, a co-simulation is believed to provide a flexible and cost-effective option for future simulations even for confidential models.

5.   Numerical prediction of material damage

In the current work material damage due to wear is accounted for. The wear generated at tread braking and in the wheel–rail contact is predicted using two separate models presented below.

5.1.   Wear and temperatures at tread braking

5.1.1.   Modelling and calibration of temperatures at tread braking

In the second part of the Vernersson's PhD thesis [20], a thermal model of railway tread braking is developed for use in routine calculations of wheel and block temperatures, including the cooling influence from the rail. Brake rig tests were performed for drag braking at constant brake power for blocks made of cast iron and sinter and organic composite materials. Results on the influence of block configuration, brake power and brake speed on wheel and block temperatures were reported. Rolling contact heat transfer from wheel to rail is studied in the brake rig using a so-called rail-wheel in contact with the braked wheel, along with results from field tests. The thermal model, a finite element (FE) model established using a commercial FE software, was calibrated by using data from experiments and can be employed to calculate temperatures and the heat partitioning between block, wheel and rail. The rail chill was found to have a considerable influence on the wheel temperature for long brake cycles. This model can be used to efficiently design tread braking systems for both freight and passenger trains. It can account for stop braking, drag braking at constant brake power as well as intermediate periods of cooling. The temperature history during a full train route can thus be calculated.

Some aspects of the work described above need further elaboration with regard to the present project. Firstly, the focus was on proper prediction of wheel behavior and thus emphasis on wheel temperatures. This meant that the model parameters were calibrated using average brake block temperatures[1] as detected by a thermocamera with a field-side view of the blocks. For the present project, where the block contact temperatures are at focus, this means that local temperature variations near-to the contact surfaces, which tentatively can be important for particle emissions, are not modelled. Secondly, the focus was on drag braking conditions, which mean low power (20-60 kW) braking having long duration (10-45 min). This means that for cases of a train route where the braking is dominated by stop braking, a different set of parametric values are required, see the PhD dissertation by Teimourimanesh [21], that particularly had stop braking in focus.

5.1.2.   Modelling and calibration of wear of friction materials

In previous work [22], an experimental study on a pin-on-disc rig was presented where the wear of some brake block materials at controlled elevated disc temperatures were reported, see Figure 2. It was found for the three studied organic composite materials that the (specific) wear rate increases radically at a temperature of about 500 ˚C. For temperatures below 500 ˚C, the wear rate was found to increase moderately with temperature. The cast iron material showed an increase of the wear rate up to 500 ˚C, after which a transition in the wear mechanism occurs and the wear rate is decreasing with increasing temperature. The studied sinter material shows a weak dependence of the wear rate with temperature. Following up on this, modelling of block wear at tread braking was explored [23], showing that for a situation of negligible thermoelastic instabilities, wear can be assessed by post-processing of temperatures calculated using a thermal only model with an assumption on nominal contact pressures and not requiring the extraneous calculation efforts required for analyzing a fully thermoelastic model.

In the present work, the wear modelling is introduced as an intrinsic part of the temperature calculation simulations. For each time increment during the temperature assessment, the wear of the brake blocks

---

[1] Average of field side of the brake block at brake rig testing as calculated using results from a thermocamera with view of the field side. For field tests, results of specific thermocouple positions were used.

are assessed using Archard's wear model. In the present study, the wear rate $\dot{w}$ [m/s] of the block is calculated in local form as

$$\dot{w} = k_{\mathrm{w}} \mu p v \tag{13}$$

where k_{w} [m^2/N] is the temperature-dependent material wear property adapted from Figure 2. The brake pressure here relates to the nominal one required for providing a wanted braking performance.
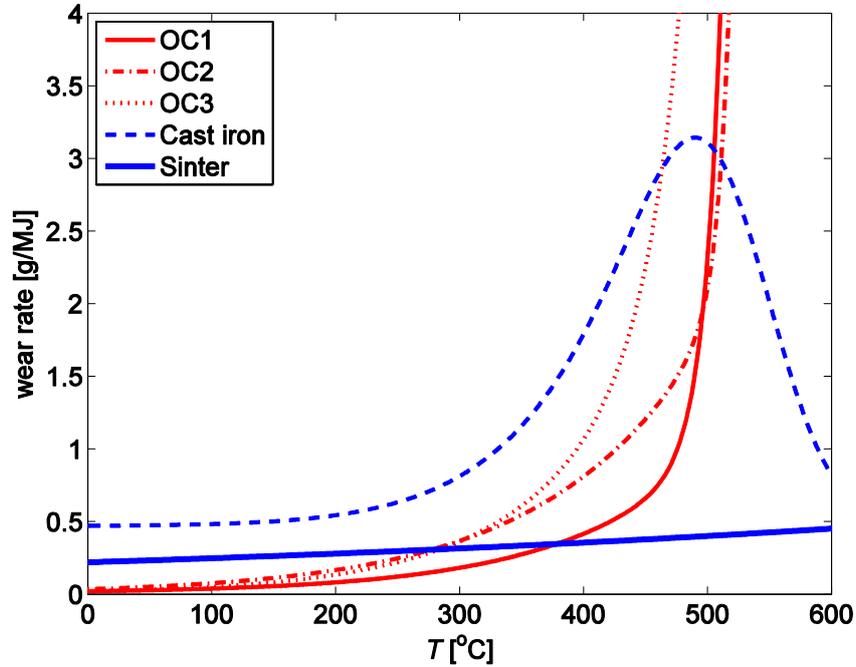
Figure 2. Measured wear rates for five brake block materials in pin-on-disc tests: organic composites OC1-OC3, cast iron and a sinter material

5.1.3.   Co-simulation with the VTI freight train simulator

The numerical model for calculation of tread braking temperatures presented in Section 5.1.1 has previously been implemented in a user-friendly Matlab code [24]. It uses the Finite Difference Method (FDM) on implicit form. The code is capable of capturing the behaviour of the FE model, and in addition it allows for easy establishment of new wheel geometries and fast analyses on a standard laptop computer, all without the need of a commercial FE software package. The wheel geometry is input to the software as a simplified wheel geometry or by using a drawing. The geometry is digitized and divided into axisymmetric control volumes by a semi-automatic approach. The simplified model can for instance account for contact resistances by controlling the heat partitioning between blocks and wheel, cooling of the wheel (from forced convection, radiation and rail chill) by using a staggered technique as well as brake power and speed variations. However, the physical properties of the wheel and brake block materials are implemented as constant, whereas in the FE model they are temperature dependent. The model used for calculation of wheel and block temperatures can be used to efficiently design tread braking systems for both freight and passenger trains. It can handle stop braking, drag braking at constant brake power, and also intermediate periods of cooling. The temperature history during a full train route can thus be calculated. However, one should note that this model was (mainly) calibrated using experimental data from drag braking experiments.

This code has within the present project been supplemented by a wear assessment module based on the modelling presented in Section 5.1.2 and it has further been modified for utilization in parallel with the train simulator software. Specifically, work has been performed to

1. modify the code for working with inputs of brake speed and brake force as provided by the simulator at each new time step and outputting the related wear and average temperature to be visualized on behalf of the simulator driver.

2. establish a suitable calculation grid density giving acceptable trade-off between time of numerical iteration and error in temperature assessment.

3. adapt the code for parallel analysis of temperatures and wear pertaining to vehicles with different braking behavior in the same train.

To this end, the code has been suitably packaged into a so-called Matlab function that, after initial set-up of calculation structures, accepts data provided by the train simulator and that within half of the chosen co-simulating time step delivers output results in terms of calculated temperatures and wear rates. It was decided that a time stepping increment of 1 s for temperature assessment would be appropriate for capturing the relatively slow variations of temperature for a tread braked vehicle.

In order to investigate the required grid density, a parametric study was initiated for studying the relation between speed of time incrementation and the error introduced. In the end, it was chosen to use an FDM grid size of 1 mm radially and 1.5 mm axially, that gave a typical error in average temperatures below 2 % and that gave an average time for a analyzing a time increment of about 0.2 s.

For a long train it would be of interest to simulate the temperatures and wear of individual wheelsets on wagons. For this reason, the code must be set-up to allow for simulation of several parallel analyses. It was found that Matlab parallel computing capabilities allows for one separate simulation per computer CPU core[2] using the chosen set-up of memory allocation.

In the present work, the actual connection between the VTI simulator and the here presented code has not been implemented but the procedure for such a connection has been discussed in Section 4.2. For demonstration and verification purpose, output data from the train simulator runs were saved in regular text files and later used for mimicking the connectivity between the two codes.

The model for assessing brake block wear can readily be expanded to also consider wheel tread wear due to block braking. Such studies are presently on-going in the CHARMEC project SD10 [25]. In addition, the modelling technique can readily be expanded to disc brakes, which with regard to the software mainly requires efforts when it comes to establishing geometries of brake disc and brake pad.

5.2.   Wear at the wheel–rail contact

Wear generated in the wheel–rail contact is calculated with a two-dimensional model that comprises four degrees of freedom. The model has been implemented in the software Simulink/Matlab. The neglection of lateral dynamics implies that differential wear of the rails for example caused due to curving is not accounted for. Calculations are performed in a post-processing step to the train simulator. The driving moment, $T_{D,ij}$, pneumatic braking moment, $T_{pB,ij}$, rolling resistance moment, $T_{R,ij}$, and the location, $x_{0,ij} + vt$ and velocity, v, of that attachment point of the primary suspension of wheel j and wagon i constitute input to the damage calculation. These are introduced by interpolation in look-up tables that hold results obtained from the train simulator.

Below, the equations of motion of wheel ij in tangential displacement, x_{ij}, vertical displacement, y_{ij}, and rotation, θ_{ii}, as well as for the rail in vertical displacement, $y_{r,ij}$, are expressed:

$$m_{ij}\ddot{x}_{ij} + c_w\dot{x}_{ij} + k_w x_{ij} = c_w v + k_w\left(x_{0,ij} + vt\right) + F_{\mu,ij} \tag{14}$$

$$m_{ij}\ddot{y}_{ij} = F_{e,ij} + m_{ij}g - F_{n,ij} \tag{15}$$

---

[2] Tests were performed on a computer equipped with a 4 core Intel i7-4770K CPU.

$$J_{ij}\ddot{\theta}_{ij} = T_{\text{D},ij} - T_{\text{pB},ij} - T_{\text{R},ij} - r_{ij}F_{\mu,ij} \tag{16}$$

$$m_{\text{r}}\ddot{y}_{\text{r},ij} + c_{\text{r}}\dot{y}_{\text{r},ij} + k_{\text{r}}y_{\text{r},ij} = F_{\text{n},ij} + m_{\text{r}}g \tag{17}$$

where m_{ij}, J_{ij} and r_{ij} are the mass, mass moment of inertia and radius of wheel ij, respectively. The damping and stiffness of the tangential primary suspension are given by c_{w} and k_{w}, respectively. The track is represented by a mass, m_{r}, suspended with damping coefficient, c_{r}, and pad stiffness, k_{r}. The vertical wheel load is represented by $F_{\text{e},ij}$.

The wheel–rail contact problem is modelled using a nonlinear Hertzian spring [26] in normal direction and Shen-Hedrick-Elkins' method [27] in tangential direction, respectively. The normal, $F_{\text{n},ij}$, and tangential, $F_{\mu,ij}$, wheel–rail contact force are obtained as:

$$F_{\text{n},ij} = k_{\text{H}}\delta^{3/2} \tag{18}$$

$$\delta = y_{ij} - y_{r,ij} - y_{\text{irr}} \tag{19}$$

$$F_{\mu,ij} = \begin{cases} (1 - (1 - v_\tau)^3)\mu F_{\text{n},ij} & v_\tau < 1 \\ \mu F_{\text{n},ij} & v_\tau \geq 1 \end{cases} \tag{20}$$

$$v_\tau = \frac{C_{11}Gabv_x}{3\mu F_{\text{n},ij}} \tag{21}$$

where k_{H} is the nonlinear Hertzian stiffness, y_{irr} is the rail irregularity, C_{11} is one of the so-called Kalker coefficient, G is the shear modulus, μ is the wheel–rail friction coefficient, a and b are the semiaxes of the contact area and v_x is the creepage.

The wheel and rail subsystems are coupled with the following constrain equations:

$$y_{ij} - \delta - y_{r,ij} = [(18)] = y_{ij} - \frac{F_{\text{n},ij}}{k_{\text{H}}\sqrt{\delta}} - y_{r,ij} = y_{\text{irr}} \tag{22}$$

$$\dot{y}_{ij} - \dot{\delta} - \dot{y}_{r,ij} = [(18)] = \dot{y}_{ij} - \frac{\dot{F}_{\text{n},ij}}{\frac{3}{2}k_{\text{H}}\sqrt{\delta}} - \dot{y}_{r,ij} = \dot{y}_{\text{irr}} \tag{23}$$

The equations of motion in Equation (14), (15) and (17) are written on matrix form. Below Equation (18) has been utilized:

$$\begin{bmatrix} m_{ij} & 0 & 0 \\ 0 & m_{ij} & 0 \\ 0 & 0 & m_{\text{r},ij} \end{bmatrix}\begin{bmatrix} \ddot{x}_{ij} \\ \ddot{y}_{ij} \\ \ddot{y}_{\text{r},ij} \end{bmatrix} + \begin{bmatrix} c_{\text{w}} & 0 & 0 \\ 0 & 0 & 0 \\ 0 & 0 & c_{\text{r}} \end{bmatrix}\begin{bmatrix} \dot{x}_{ij} \\ \dot{y}_{ij} \\ \dot{y}_{\text{r},ij} \end{bmatrix} + \begin{bmatrix} k_{\text{w}} & 0 & 0 \\ 0 & 0 & 0 \\ 0 & 0 & k_{\text{r}} \end{bmatrix}\begin{bmatrix} x_{ij} \\ y_{ij} \\ y_{\text{r},ij} \end{bmatrix}$$
$$= \begin{bmatrix} c_{\text{w}}v + k_{\text{w}}(x_{0,ij} + vt) \\ F_{\text{e},ij} - k_{\text{H}}\delta^{3/2} \\ m_{\text{r},ij}g + k_{\text{H}}\delta^{3/2} \end{bmatrix} \tag{24}$$

The second-order differential equation of Equations (16) and (24) are transformed to first-order form suitable for ordinary differential equation solvers. A state vector $\mathbf{z}(t)$ is constructed that contains a mix of physical degrees of freedom and a force:

$$\mathbf{z}(t) = [x_{ij} \quad y_{ij} \quad y_{\text{r},ij} \quad \dot{x}_{ij} \quad \dot{y}_{ij} \quad \dot{y}_{\text{r},ij} \quad \dot{\theta}_{ij} \quad F_{\text{n},ij}]^{\text{T}} \tag{25}$$

The system matrices are assembled from Equations (24), (16), (20) and (22)-(23) as:

$$\mathbf{A}\dot{\mathbf{z}} + \mathbf{B}\mathbf{z} = \mathbf{Q} \tag{26}$$

$$\mathbf{A} = \begin{bmatrix}
c_{\mathrm{w}} & 0 & 0 & m_{ij} & 0 & 0 & 0 & 0 \\
0 & 0 & 0 & 0 & m_{ij} & 0 & 0 & 0 \\
0 & 0 & c_{\mathrm{r}} & 0 & 0 & m_{\mathrm{r}} & 0 & 0 \\
1 & 0 & 0 & 0 & 0 & 0 & 0 & 0 \\
0 & 1 & 0 & 0 & 0 & 0 & 0 & 0 \\
0 & 0 & 1 & 0 & 0 & 0 & 0 & 0 \\
0 & 0 & 0 & 0 & 0 & 0 & J_{ij} & 0 \\
0 & -1 & 1 & 0 & 0 & 0 & 0 & 1/\left(\frac{3}{2}k_{\mathrm{H}}\sqrt{\delta}\right)
\end{bmatrix} \tag{27}$$

$$\mathbf{B} = \begin{bmatrix}
k_{\mathrm{w}} & 0 & 0 & 0 & 0 & 0 & 0 & 0 \\
0 & 0 & 0 & 0 & 0 & 0 & 0 & 1 \\
0 & 0 & k_{\mathrm{r}} & 0 & 0 & 0 & 0 & -1 \\
0 & 0 & 0 & -1 & 0 & 0 & 0 & 0 \\
0 & 0 & 0 & 0 & -1 & 0 & 0 & 0 \\
0 & 0 & 0 & 0 & 0 & -1 & 0 & 0 \\
0 & 0 & 0 & 0 & 0 & 0 & 0 & (1-(1-v_\tau)^3)\mu r_{ij} \\
0 & -1 & 1 & 0 & 0 & 0 & 0 & 1/k_{\mathrm{H}}\sqrt{\delta}
\end{bmatrix} \tag{28}$$

$$\mathbf{Q} = \begin{bmatrix}
c_{\mathrm{w}}v + k_{\mathrm{w}}\left(x_{0,ij} + vt\right) + F_{\mu,ij} \\
F_{\mathrm{e},ij} + m_{ij}g \\
m_{\mathrm{r}}g \\
0 \\
0 \\
0 \\
T_{\mathrm{D},ij} - T_{\mathrm{pB},ij} - T_{\mathrm{R},ij} \\
-y_{\mathrm{irr}} - \dot{y}_{\mathrm{irr}}
\end{bmatrix} \tag{29}$$

Figure 3. Model used for simulation of damage in the wheel–rail contact

5.2.1. Calculation of rail wear

The wear generated in the wheel–rail contact is calculated using the so-called "friction-work" or $T\gamma$-model [28]. This assumes that the material removal is proportional to the dissipated energy in the contact area. The ware rate w [kg/m/mm^2] corresponding to the removed mass per metre rolled distance and per mm^2 of the contact area is expressed as:

$$w = K\frac{T\gamma}{A}$$

(30)

where K is a model coefficient, A [mm^2] is the wheel–rail contact area and $T\gamma$ [N] is the wear index calculated as the product of the tangential contact force, T, and the resulting creepage, γ, in the wheel–rail contact area. In this work the tangential contact force, T, corresponds to F_μ in Section 5.2 . Twin-disc experiments by Bolton and Clayton [29] illustrated the rate at which wear was generated to vary significantly with the wear index. This observation illustrated that wear generation occurs at different regimes; mild, severe and catastrophic. Amongst others, these regimes are associated with different proportionality constant between wear rate and wear index. Wear rates obtained by twin-disc experiments for a 260 rail grade and R8T wheel material are presented in [30], see Figure 4. The mild wear regime is characterized by proportionality between wheel rate and the friction work. This is shown for friction work below approximately 4 N/mm^2 in the results presented for dry wheel–rail contact in Figure 4. The maximum friction work magnitudes ($T\gamma/A$) simulated in the current work has been found to be below 1 N/mm^2. According to Figure 4, this corresponds to wear generation in the mild regime. The wear rate is modelled according to Equation (30) with $K = 2.25$ [μg/mN]. This project serves the purpose of demonstrating new simulation capabilities rather than to make quantitative assessments of e.g. damage. Hence, the specific choice of wheel and rail materials and their associated wear coefficient is of minor importance.

Figure 4. Wear rates measured by twin-disc experiments for 260 rail grade and R8T wheel material [30]

6.   Results

The new functionality of the freight train simulator for prediction of damage at brakes and in the wheel–rail contact is demonstrated for a selected test track section between the Swedish cities Forserum – Tenhult – Huskvarna – Jönköping. The simulated train has length 619 m and a total mass of 2 782 tonnes. It consists of one Traxx locomotive [31] and 30 freight wagons of mass 82 tonnes and 18.5 tonnes, respectively. In addition, each freight wagon carries a load of 71.5 tonnes. The wheel radius and mass moment of inertia of the locomotive and the wagons are 0.6 m and 0.4 m, and 615 kgm² and 139 kgm², respectively. The radius of the transverse rail profile used in the calculation of normal wheel–rail contact is assumed to be 0.3 m. In combination with the wheel radius of the locomotive and the wagons, Hertzian contact theory results in wheel–rail contact areas equal to 140 mm² and 30.3 mm², respectively. The wear generated in the wheel–rail contact is modelled as proportional to the frictional work with proportionality constant $K = 2.25$ [μg/mN]. In this section, the damage predicted for simulations by an experienced train driver is compared towards that obtained for a vehicle that provokes the automatic train control system (ATC).

6.1.   Selected track section: Forserum - Jönköping

Selected properties of the track alignment for the simulated track section is presented in Figure 5. The distribution of track lengths on different ranges of curve radii is shown in Figure 6. The travel from Forserum to Jönköping corresponds to a track length of 27 km and a reduction in altitude of 190 m, see Figure 5. The maximum speed limit is 130 km/h. From Figure 6 it is observed that approximately half of the track length belongs to curves with radii smaller than 1500 m. Moreover, approximately one third of the total simulated stretch consists of tangent track.
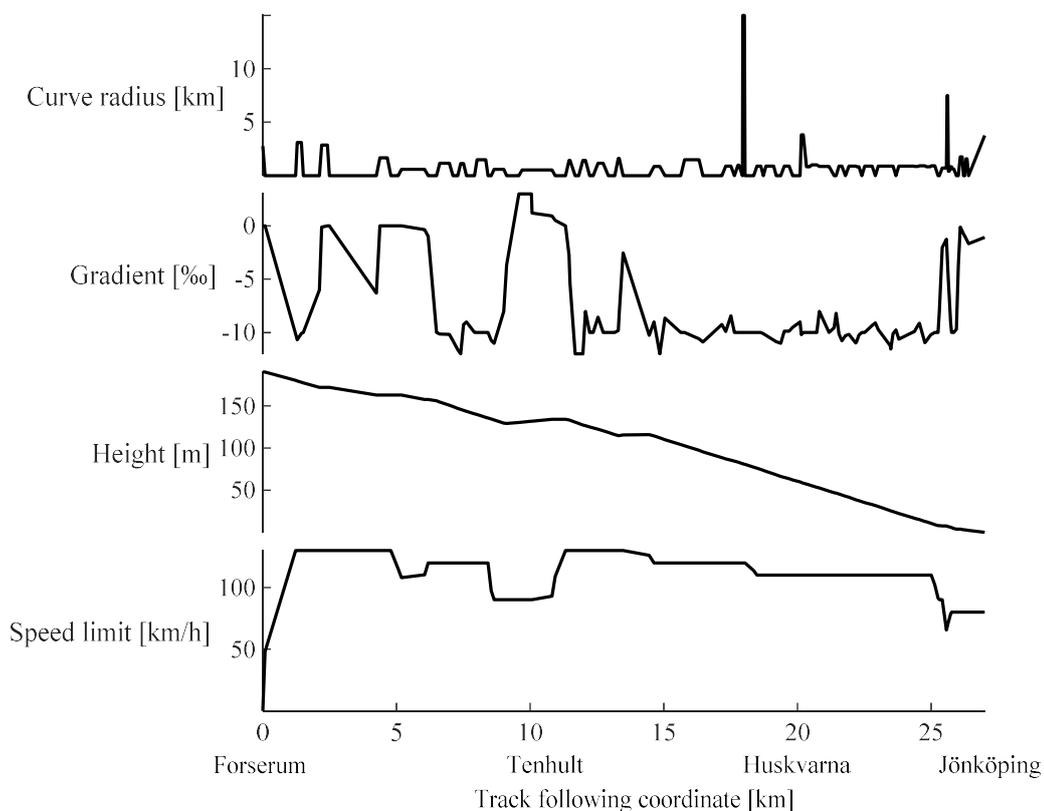
Figure 5. Selected properties of the track alignment presented for the simulated track section between Forserum – Jönköping. From top to bottom the figures show; (1) curve radius, (2) vertical gradient, (3) track height and (4) speed limit

21
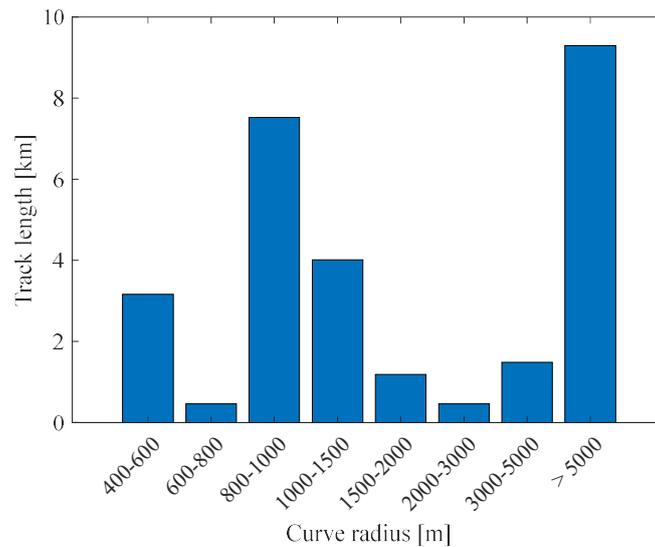
Figure 6. Track length distributed over different curve radius ranges

6.2.   Predictions of damage

6.2.1.   Wheel–rail wear

The wear generated at the tread brakes and in the wheel–rail contacts is calculated for simulation of the freight train between Forserum and Jönköping. Results obtained for an experienced train driver (hereafter termed "normal driving") and a driver that provokes the automatic train control system (hereafter termed "ATC driving") are compared. In Figure 7 the two train journeys are presented in terms of the mechanical energy insert through traction applied by the locomotive and the energy dissipated due to friction braking. It should be noted that the travel from Forserum to Jönköping corresponds to a height difference of 190 m which, for the current train, equals a potential energy of approximately 5 GJ. Results simulated for ATC driving exceeds those for normal driving both with respect to the input and dissipation of energy, see Figure 7. The accumulated energy dissipated through the tread brakes during ATC driving is 32 % higher compared to that simulated for Normal driving. The wear caused by the wheel–rail contacts are presented in Figure 8. The accumulated mass of the wear caused during ATC driving exceeds that for normal driving with 38 %.
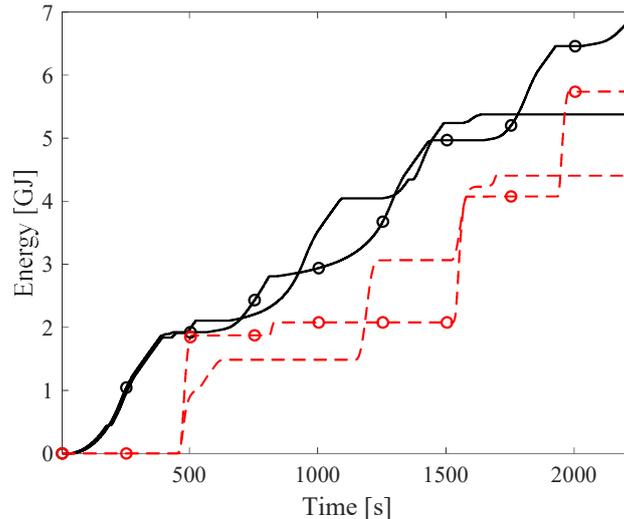
Figure 7. Accumulated mechanical energy insert and consumption during simulation between cities Forserum and Jönköping. Energy insert through traction of the locomotive during normal (—) and ATC (–o–) driving. Energy consumed by friction braking during normal (– –) and ATC (–o–) driving
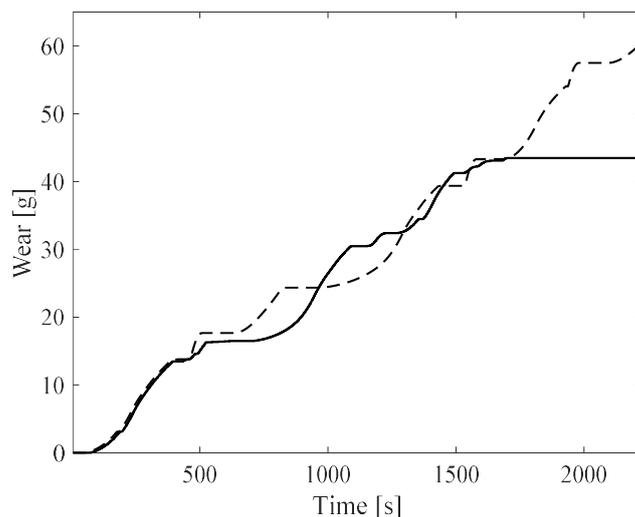
Figure 8. The accumulated wear generated by the wheel–rail contacts during simulation between cities Forserum and Jönköping. —: Normal driving, – –: ATC-driving

6.2.2. Tread braking temperatures and wear

In the following, the wear and elevated temperatures calculated for the tread brakes are presented and discussed. It should be noted that in the actual implementation in the VTI simulator, real-time temperatures and wear data will be visualized to the driver, thus providing immediate feed-back on her/his driving actions. A proposal for such an on-screen real-time presentation, already implemented in the updated software, is presented in Figure 9. Possibly could also accumulated wear on each wagon be indicated to the driver and even a predicted total accumulated wear considering all wagons of the train.
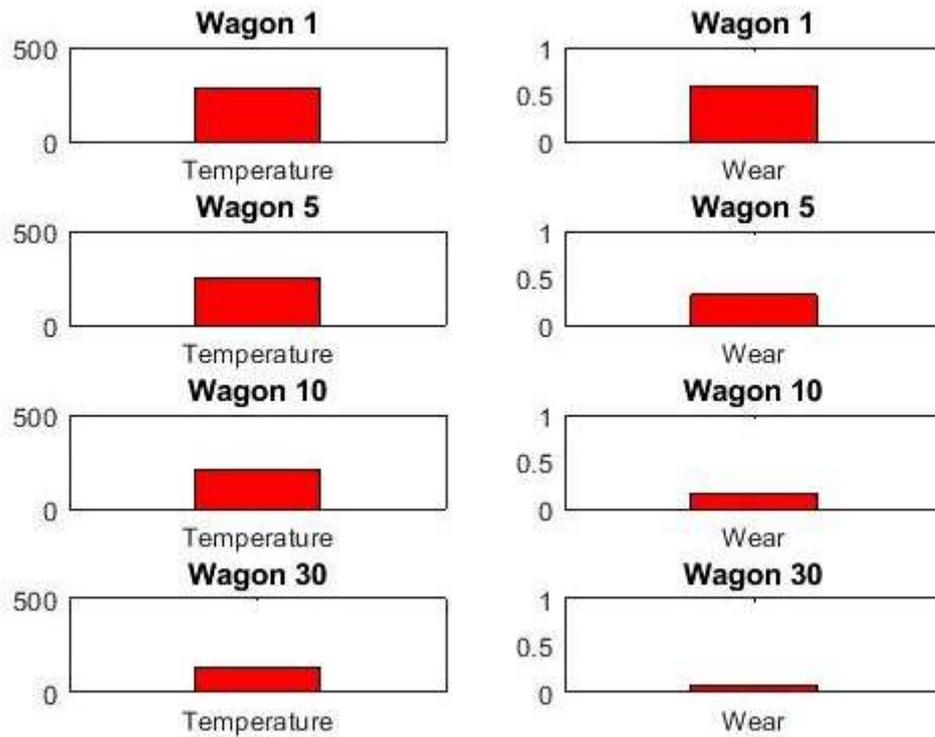
Figure 9. Tentative approach of presenting temperatures [°C] and wear [g/s] for 4 chosen wagons in the train. Example is from one chosen time increment during a stopping of the studied train

Brake temperatures are presented in Figure 10 and wear on four wagons of the train are presented in Figure 11. The two cases are chosen to provide rather extreme cases of locomotive driver behavior for giving an indication of driver influence on temperatures and wear. It is evident that the train driving behavior has an impact on wheel and brake block contact temperatures, with an increase of highest temperature on block from 480 °C to 600 °C and a corresponding increase in maximum wheel temperatures from 370 °C to 440 °C. This increase in temperatures is also reflected in the maximum block wear rates during the route, increasing from 0.62 g/s to 1.05 g/s. These differences in wear are more clearly shown by the accumulation of wear as given in Figure 12. The total calculated wear for the four wagons is 99 g for the normal driving case and 179 g for the ATC driving case. The ATC driving case results in almost a doubled amount of wear as compared to normal driving. The graph also provides an overview of the variation of the wear within the train, with the highest wear is found near the locomotive and the lowest wear at the back of the train. This is a result of a delay in the braking action that increases with the length of the pneumatic braking system.
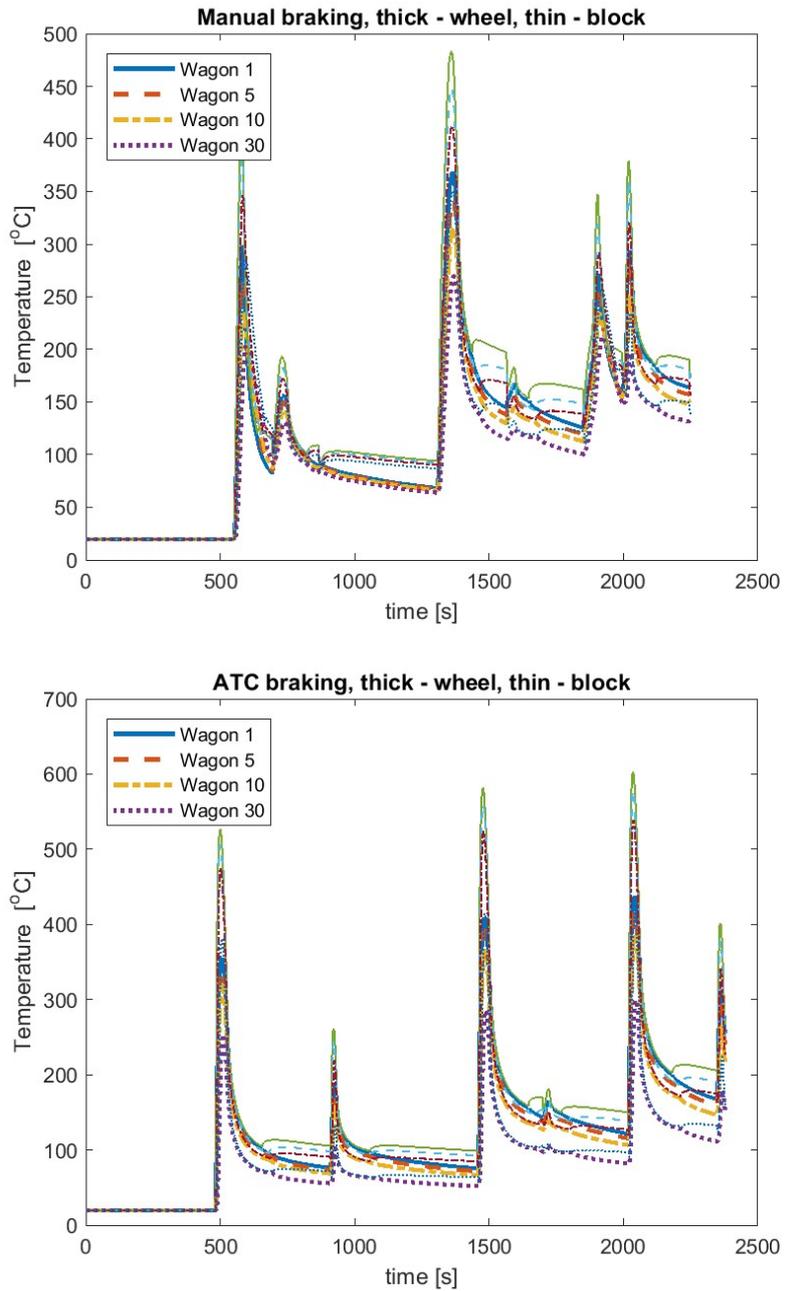
Figure 10. History of calculated braking temperatures for the test track Forserum – Tenhult – Huskvarna – Jönköping. Upper figure is standard brake operation (normal driving) and lower is for the case when the ATC system controls the brake (ATC driving)
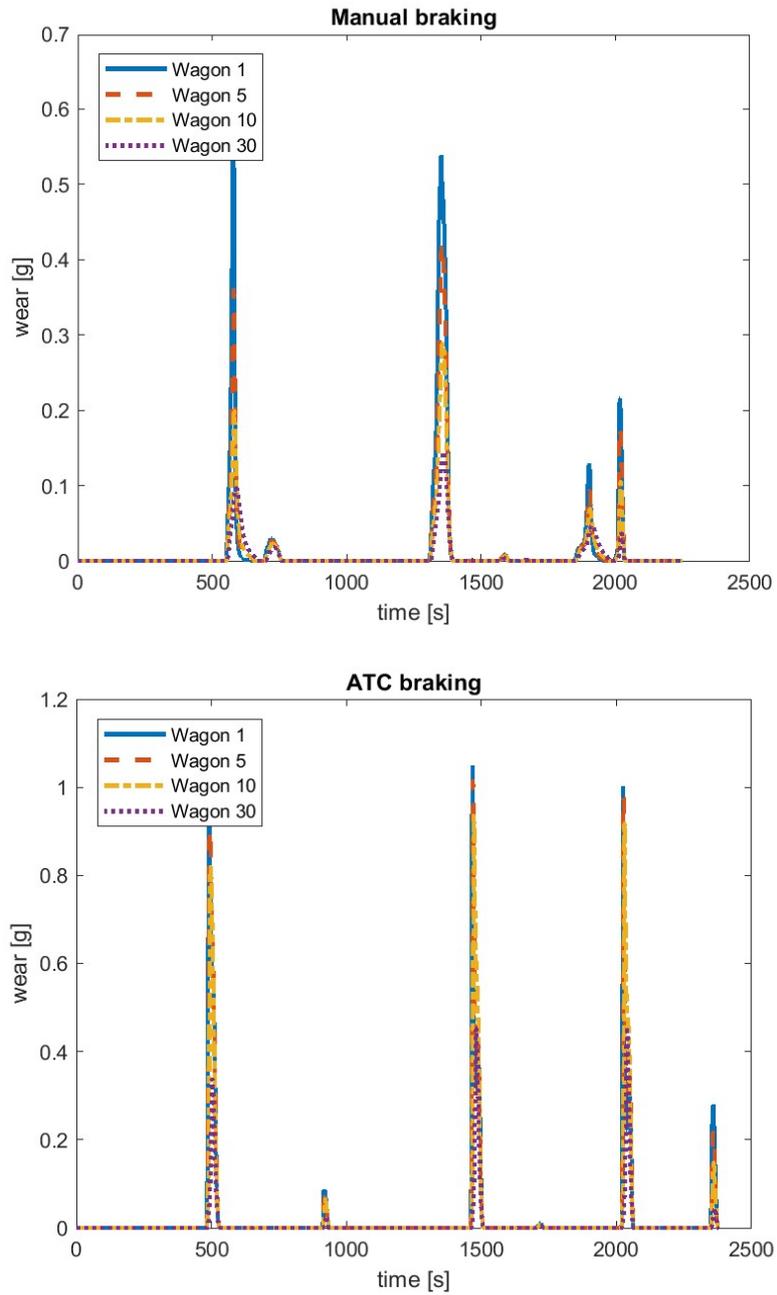
Figure 11. History of calculated wear for the test track Forserum – Tenhult – Huskvarna – Jönköping. Upper figure is standard brake operation (i.e. normal driving) and lower is for the case when the ATC system controls the brake (ATC driving)
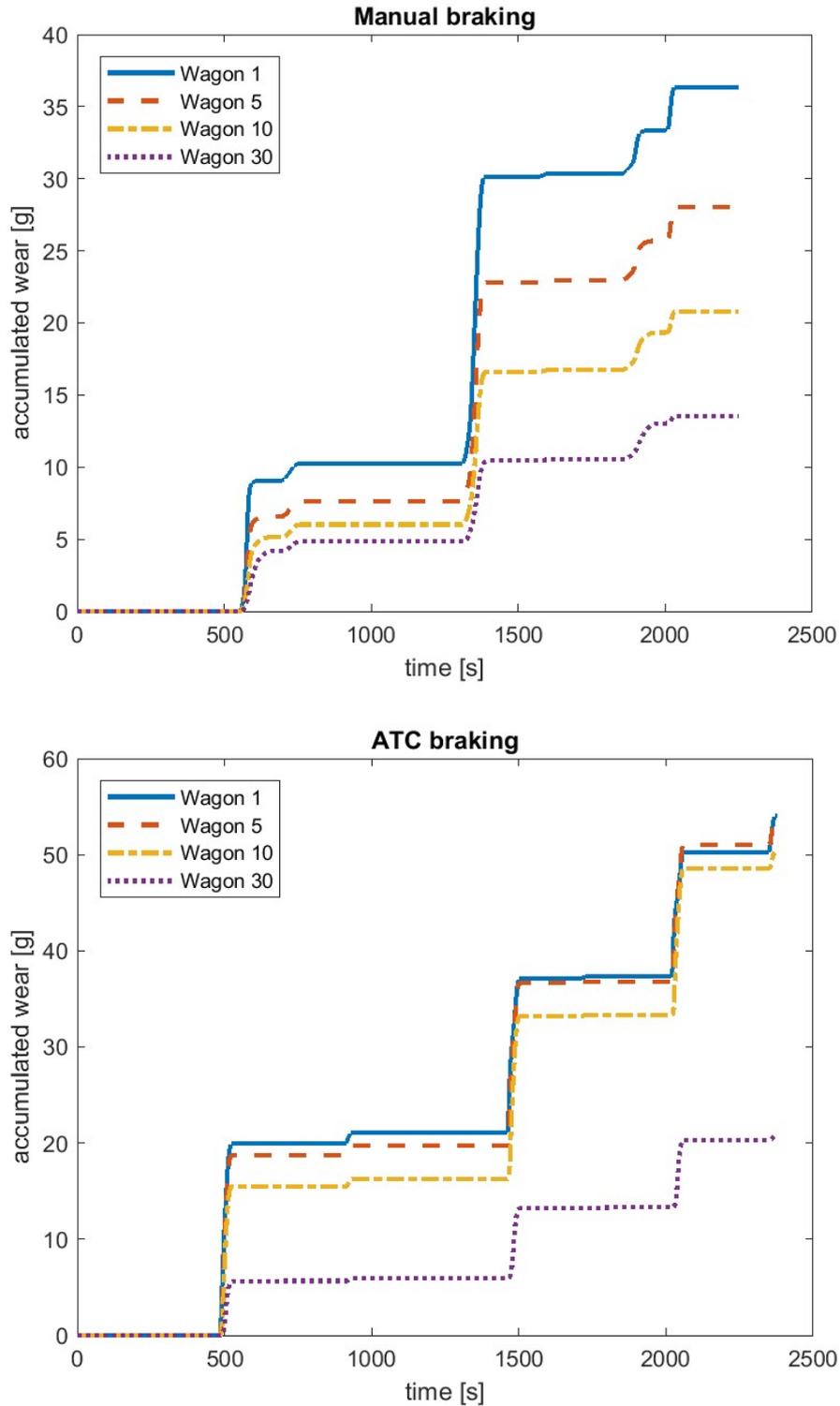
Figure 12. Calculated accumulated wear for the test track Forserum – Tenhult – Huskvarna – Jönköping. Upper figure is standard brake operation (normal driving) and lower is for the case when the ATC system controls the brake (ATC driving)

6.2.3. Tread braking – study of local contact temperatures

The modelling and calibration work regarding tread braking temperatures have relied on the assessment of average temperatures, as described in Section 5.1.1. Tentatively, local temperature variations in the block contact could be important for the particle emissions that are generated at braking, e.g. when it

comes to the relation between mass wear and distribution of particle sizes. Revisiting brake rig test data produced by a thermocamera during Vernersson's PhD work, where the brake block field side temperatures were captured by the thermal imaging system, it can preliminary be concluded that the local temperatures near the contact exhibit substantial variations, see Figure 13. For the assessed stop braking cycles these results indicate that the local temperature[3] can be up to 50 times higher than the average temperature for cast iron brake blocks, and 5 and 1.5 times higher respectively for a sinter material block and an organic composite brake block. These temperature variations are to a large extent produced by frictionally induced thermoelastic instabilities both pertaining to the wheel tread and to the brake block, see also [32]. The results indicate that there are reasons to further develop the current predictions of block temperatures so that the range of resulting contact temperatures is represented. It is anticipated that contact temperatures are important for the size and morphology of particles resulting from braking.

---

[3] Here represented by temperatures on the field side of the brake block some 5 mm away from the tread contact
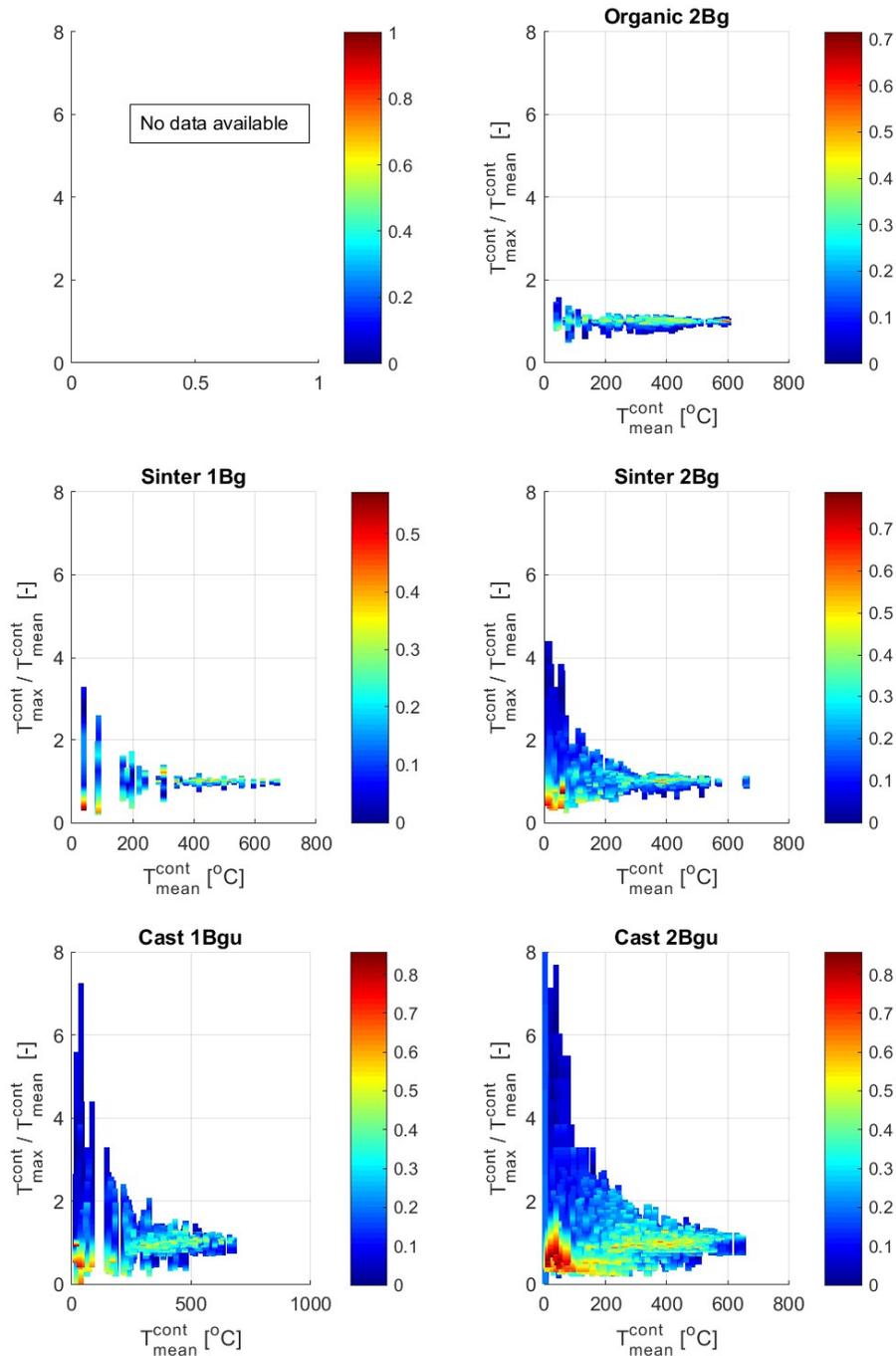
Figure 13. Assessment of variation of block temperatures near contact interface as represented by temperatures detected using thermal imaging on field side of block at distance 5 mm from tread contact. For each time instant for which block temperatures are acquired, one vertical (colored) line is introduced in the figure at the calculated average temperature. The line starts at the ratio of minimum local temperature over average temperature and ends at the same ratio for maximum temperature. The color variation inside the line indicates how common the different ratios of temperatures are calculated as the number of occurrences inside a part of the temperature range as compared to total number of occurrences

6.2.4. Procedure for mapping of railway non-exhaust particle emissions

As part of the current work a procedure to visualize results obtained in the train simulator on a map published on an internet webpage has been developed, see Figure 14. The procedure is generally applicable in the sense that any quantity calculated during simulation in the train simulator can be

transfer to the corresponding locations along the considered railway line on the map. Figure 14 demonstrates this visualization technique by showing brake force magnitudes. The large magnitude brake forces (which corresponds to increased magnitudes of the generated wear) at Huskvarna is noticed.
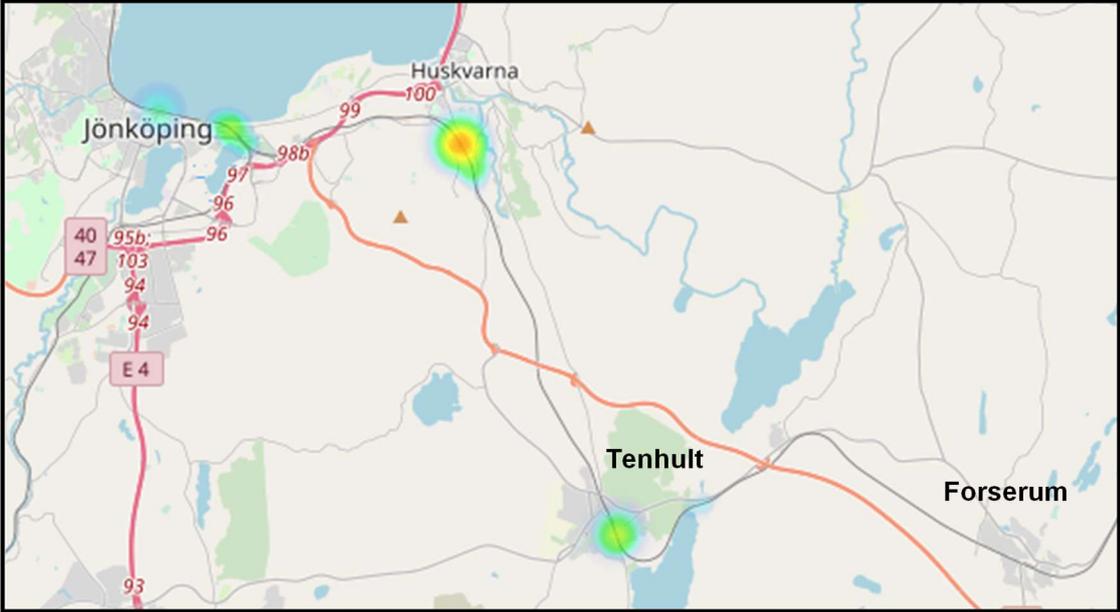
Figure 14. Example view of the web-based visualization procedure developed as part of the current project. Here braking forces are shown

7.   Concluding remarks

This feasibility study is an interdisciplinary collaboration between three research institutes (VTI, Chalmers University of Technology and RISE) and a railway brake manufacturer (Faiveley Transport Nordic). Senior researchers specialized on numerical modelling of friction brakes respective particle matters (PM), are combined with expertise in the field of train driving simulations to reduce railway's impact on environment and human health. The train driving simulator of VTI is further developed to account for the wear generated at the brake blocks and in the wheel–rail contact.

A literature study that focuses on prediction of non-exhausted railway particle emissions is presented. The particle emissions from railway wear originates from both the wheel–rail and brake block–wheel contact. In this study contacting surfaces are assumed to be manufacture from metal. The particle emissions are for some size classes related to the wear volume, i.e. the coarse and occasionally the fine particles as well, while the ultrafine particle, i.e. smaller than 100 nm, are too small to give a noticeable effect on wear volume. From pin-on-disc studies particles of size 350 nm are common, but for all given diameters one needs to make sure that the same diameter definition is used, as this information is sometimes difficult to find in literature. The emissions of wear particles need to be modelled with more information from the wear model than does the wear volume. This is because temperature, pressure and relative velocity in the contact have a significant impact on particle size and type of wear.

Damage due to wear is calculated in a post-processing step to the train simulator. The longitudinal dynamic vehicle–track interaction is accounted for by a two-dimensional model developed and implemented in the software Simulink/Matlab. This model simulates the dynamic interaction between each wheel of a train separately. Simulations are performed for a prescribed static vertical wheel load, wheel rotational velocity, and location and velocity of the mounting point of the primary suspension on the bogie frame. The wheel–rail contact problem is modelled using a nonlinear Hertzian spring in normal direction and Shen-Hedrick-Elkins' method in tangential direction, respectively. The generation of wear is assumed to be proportional to the work performed by the friction forces.

A novel module for visualizing braking temperatures and brake block wear has been implemented for providing real-time information to the simulator driver. The module is prepared for being directly connected to the main computer of the VTI simulator. Based on data from the simulator, temperatures of wheels and brake blocks of a number of wagons are continuously calculated using a detailed finite difference model of wheels and blocks that accounts for cooling by convection and radiation, but also considering the cooling influence on the wheel introduced by the continuous rolling contact with the cold rail. The wear of the brake blocks is assessed using Archard´s wear model, where the wear rate parameter is temperature dependent.

The new functionality for prediction of wear generation is demonstrated for the railway line between cities Forserum – Tenhult – Huskvarna – Jönköping located in the province Småland, Sweden. A freight train with length 619 m and total mass 2 782 tonnes is simulated. Results obtained for an experienced driver is compared to those simulated with an aggressive train driving behavior that activates the Automatic Train Control (ATC) system. For the aggressive driving behavior, the worn off mass generated in the wheel–rail contacts are found to be approximately 38 % larger compared to that by the experienced driver and similarly for the brake blocks the wear is 81 % larger for the ATC braking case.

A method to visualize results obtained in the train simulator on a map has been developed. The procedure is web-based meaning that the results are presented on an internet webpage. The procedure is generally applicable in the sense that any quantity calculated during simulation in the train simulator can be presented. This functionality is believed to become useful in future attempts to identify so-called hot-spots corresponding to locations along the track network exposed to increased levels of particle emissions.

References

1. Prognos över svenska godsströmmar år 2050 [Internet]. Trafikverket; 2012. Available from: https://trafikverket.ineko.se/Files/sv-SE/10772/RelatedFiles/2012_112_Prognos_over_svenska_godsstrommar_ar_2050.pdf

2. Karlsson A. Allt färre bor i glesbygd. Välfärd [Internet]. 2012; Available from: https://www.scb.se/statistik/_publikationer/le0001_2012k02_ti_04_a05ti1202.pdf

3. Infrastruktur för framtiden – innovativa lösningar för stärkt konkurrenskraft och hållbar utveckling [Internet]. Regeringens proposition 2016/17:21; 2016. Available from: https://www.regeringen.se/4a8e11/contentassets/569a9026b427483fbfca847f66dd27e5/infrastruktur-for-framtiden--innovativa-losningar-for-starkt-konkurrenskraft-och-hallbar-utveckling-prop-20161721.-.pdf

4. Förslag till nationell plan för transportsystemet 2018–2029, Remissversion 2017-08-31 [Internet]. Trafikverket; 2017. Available from: https://trafikverket.ineko.se/se/förslag-till-nationell-plan-för-transportsystemet-2018-2029-remissversion-2017-08-31-2

5. Analysmetod och samhällsekonomiska kalkylvärden för transportsektorn [Internet]. Trafikverket. 2019. Available from: https://www.trafikverket.se/asek

6. Gustafsson M, Abassi S, Blomqvist G, Cha Y, Gudmundsson A, Janhäll S, et al. Particles in road and railroad tunnel air: sources, properties and abatement measures. VTI; 2016. Report No.: 917A.

7. Fridell E, Ferm M, Ekberg A. Emissions of particulate matters from railways – Emission factors and condition monitoring. Transp Res Part Transp Environ. 2010;15(4):240–5.

8. Park JH, Young Woo H, Chuel Park J. Major factors affecting the aerosol particulate concentration in the underground stations. Indoor Built Environ. 2012;23(5):629–39.

9. Grassie SL, Elkins JA. Tractive effort, curving and surface damage of rails: Part 1. Forces exerted on the rails. Wear. 2005;258(7–8):1235–44.

10. Karlsson HL, Nilsson L, Möller L. Subway particles are more genotoxic than street particles and induce oxidative stress in cultured human lung cells. Chem Res Toxicol. 2005 Jan 1;18(1):19–23.

11. Gustafsson M, Blomqvist G, Gudmundsson A, Dahl A, Swietlicki E, Bohgard M, et al. Properties and toxicological effects of particles from the interaction between tyres, road pavement and winter traction material. Sci Total Environ. 393(2):226–40.

12. Hinds WC. Aerosol technology: properties, behavior, and measurement of airborne particles. New York: Wiley; 1999.

13. Olofsson U, Zhu Y, Abbasi S, Lewis R, Lewis S. Tribology of the wheel–rail contact – aspects of wear, particle emission and adhesion. Veh Syst Dyn. 51(7):1091–120.

14. Olofsson U, Sundvall K. Influence of leaf, humidity and applied lubrication on friction in the wheel-rail contact: Pin-on-disc experiments. Proc Inst Mech Eng Part F J Rail Rapid Transit. 218(3):235–42.

15. Lee H, Namgung H-G, Kwon S-B. Effect of train velocity on the amount of airborne wear particles generated from wheel–rail contacts. Wear. 414–415:296–302.

16. Liu H, Cha Y, Olofsson U, Jonsson LTI, Jönsson PG. Effect of the sliding velocity on the size and amount of airborne wear particles generated from dry sliding wheel–rail contacts. Tribol Lett. 63(3):30.

17. Abbasi S, Wahlström J, Olander L, Larsson C, Olofsson U, Sellgren U. A study of airborne wear particles generated from organic railway brake pads and brake discs. Sel Pap 14th Nord Symp Tribol Nord 2010. 2011 Nov 1;273(1):93–9.

18. Andersson A, Kharrazi S. Freight train model for real time simulation. In Rockhampton, Queensland, Australia; 2017.

19. Wall E. Physical modelling of railway vehicles for real-time simulation [Master's thesis report]. [Stockholm]: Royal Institute of Technology (KTH); 2006.

20. Vernersson T. Tread braking of railway wheels - Noise-related tread roughness and dimensioning wheel temperatures [Ph.D. Dissertation]. [Göteborg]: Chalmers University of Technology; 2006.

21. Teimourimanesh S. Thermal capacity of railway wheels - temperatures, residual stresses and fatigue damage with special focus on metro applications [Ph.D. Dissertation]. [Göteborg]: Chalmers University of Technology; 2013.

22. Vernersson T, Lundén R, Abassi S, Olofsson U. Wear of railway brake block materials at elevated temperatures: pin-on-disc experiments. In: Proceedings of Eurobrake 2012, FISITA. Dresden, Germany; 16-18 April.

23. Vernersson T, Lundén R. Wear of brake blocks for in-service conditions—Influence of the level of modelling. Wear. 2014;314(1):125–31.

24. Vernersson T. Tread braking of railway wheels - dimensioning wheel temperatures, Software manual version 1.0. Chalmers University of Technology;

25. Chalmers Railway Mechanics (CHARMEC) [Internet]. Available from: www.charmec.chalmers.se

26. Hertz H. Über die berührung fester elastischer Körper. J Für Reine Angew Math. 1882;92:156–71.

27. Shen ZY, Hedrick JK, Elkins JA. A comparison of alternative creep force models for rail vehicle dynamic analysis. Veh Syst Dyn. 1983;12(1–3):79–83.

28. Ward A, Lewis R, Dwyer-Joyce RS. Incorporating a railway wheel wear model into multi-body simulations of wheelset dynamics. Wear. 2003;41:367–76.

29. Bolton PJ, Clayton P. Rolling-sliding wear damage in rail and tyre steels. Wear. 1984;93(2):145–65.

30. Hardwick C, Lewis R, Eadie DT. Wheel and rail wear—Understanding the effects of water and grease. In: Proceedings of the 9th International Conference on Contact Mechanics and Wear of Rail/Wheel Systems. Chengdu, China; 2012. p. 198–204.

31. Bombardier Transportation [Internet]. 2018. Available from: https://www.bombardier.com/

32. Thuresson D. Thermomechanics of block brakes [Ph.D. Dissertation]. [Göteborg]: Chalmers University of Technology; 2006.